Morphological Evolution and Weak Interface Development within CVD-Zirconia Coating Deposited on Hi-Nicalon Fiber*

Hao Li, Jinil Lee, Matthew R. Libera, and Woo Y. Lee#, +
Department of Chemical, Biochemical and Materials Engineering
Stevens Institute of Technology, Hoboken, NJ 07030

Anteneh Kebbede#
General Electric Corporate Research & Development, Niskayuna, NY 12309

Michael J. Lance#
Oak Ridge National Laboratory, Oak Ridge, Tennessee 37831-6068

Hongyu Wang
General Electric Power System, Schenectady, NY 12345

Gregory N. Morscher
Ohio Aerospace Institute, c/o NASA Glenn Research Center, MS 106-01, Cleveland, OH 44135

* Supported by NSF (DMR-GOALI 9971623) with co-funding from Air Force Research Laboratory (AFRL).

Member of American Ceramic Society.

+To whom all correspondence should be addressed.

Abstract

The phase contents and morphology of a ZrO_2 fiber coating deposited at 1050°C on Hi-Nicalon^{TM} by chemical vapor deposition were examined as a function of deposition time from 5 to 120 min. The morphological evolution in the ZrO_2 coating was correlated to the development of delamination within the ZrO_2 coating. The delamination appears to occur as a result of: (1) continuous formation of tetragonal ZrO_2 nuclei on the deposition surface; (2) martensitic transformation of the tetragonal phase to a monoclinic phase upon reaching a critical grain size; and (3) development of significant compressive hoop stresses due to the volume dilation associated with the transformation. Our observations suggest that it will be of critical importance to further understand and eventually control the nucleation and grain growth behavior of CVD ZrO_2 and its phase transformation behavior for its potential applications for composites.

I. Introduction

Unlike traditional brittle ceramic materials, SiC/SiC composites are made to be tough and damage tolerant by incorporating a weak fiber coating (e.g., BN), which can deflect cracks and promote debonding at the fiber/matrix interface region. However, the BN fiber coating, while it provides superior weak interface behavior, has proved to be susceptible to oxidation from about 700 to 1000°C. This oxidation problem, which is commonly referred to as "pesting," is considered to be one of the major problems remaining to be solved before SiC/SiC composites can be reliably introduced into next-generation aircraft engines, power generation gas turbines, space vehicles, and other industrial applications.[1]

Recently, Lee et al.[2] reported that SiC/SiC minicomposite specimens containing a $SiO_2/ZrO_2/SiO_2$ multilayer coating prepared by chemical vapor deposition (CVD) exhibited graceful tensile failure behavior and extensive crack deflection within the multilayer interface region.[2] The minicomposite possessed a reasonable degree of load-carrying capability and retained much of the composite characteristics after short-term exposure to pesting conditions. The inner SiO_2/ZrO_2 interface was found to be the weakest interface in the multilayer coating region. Initially, it was speculated that the significant coefficient of thermal expansion (CTE) mismatch might result in the development of extreme residual strains and consequent "weakening" of the interfaces of the multilayer coating.

A possible role of ZrO_2 phase transformation on the apparent weak interface behavior was not included in Lee et al.'s[2] discussion of the experimental observations. It is well known that various applications of ZrO_2 stem from its polymorphism and martensitic phase transformation behavior. The martensitic phase transformation of ZrO_2 from *t* (tetragonal) to *m* (monoclinic) is accompanied by significant volume dilation and shear.[3] If the *t*-to-*m*

transformation occurred in the multilayer coating during the CVD synthesis or cooling, the volume change associated with the transformation would result in the development of significant hoop compressive stresses in the ZrO_2 coating. This might cause the ZrO_2 layer to delaminate from the SiO_2 layer. The objective of this study was to carefully examine the phase content and morphology of the CVD-ZrO_2 coating as a function of deposition time (i.e., coating thickness) by transmission electron microscopy (TEM) and Raman microscopy in order to assess the role of the phase transformation on the apparent weak interface observed in the $SiO_2/ZrO_2/SiO_2$ multilayer coating.

II. Experimental

Six CVD-ZrO_2 coating specimens were prepared at different deposition times: 5, 10, 20, 30, 60, and 120 min. A hot-wall CVD reactor was used for ZrO_2 deposition. As schematically shown in Figure 1, the reactor chamber was made of a fused SiO_2 tube (3.4 cm outside diameter and 34 cm length). A long Hi-Nicalon^{TM} fiber tow (Nippon Carbon Co., Ltd., Japan) was wrapped around a fused SiO_2 holder to make about 9 fiber tow specimens (~24 cm long) for each deposition experiment.

The reactor was heated using a resistance furnace with an effective heating zone of about 30 cm. The temperature at the center region of the reactor was measured and controlled using a K-type thermocouple interfaced to a temperature controller. The pressure inside the reactor chamber was controlled using a mechanical vacuum pump and an exhaust valve (Type 253, MKS, Waltham, MA) interfaced to a pressure controller (Type 252A, MKS) and a capacitance manometer (Baratron, MKS). The reactor was operated using $ZrCl_4$, CO_2, and H_2 as precursors at a temperature of 1050°C and a pressure of 4 kPa for the CVD experiments.

A 500 cm^3 stainless steel vaporizer was used to hold $ZrCl_4$, which is a solid at room temperature. The vaporizer was kept at a constant temperature of 190°C using heating tapes to maintain the vapor pressure of $ZrCl_4$. An Ar stream was used to carry the $ZrCl_4$ vapor from the vaporizer to the reactor chamber. The flow rates of Ar, H_2, and CO_2 were controlled by mass flow meters (Type 258, MKS, Andover, MA): 40 cm^3/min for Ar, 120 cm^3/min for H_2, and 120 cm^3/min for CO_2 at STP.

Tensile tests were conducted at room temperature. The length of fiber tow specimens was 20 cm. The entire length of each fiber tow specimen was glued to a plastic strip (20 cm x 2 cm x 0.1 mm) using a 5-min epoxy, except for the 2.5 cm gauge length. At least five tows were tested for each condition. Also, for comparison, 5 flame-desized fiber tows were tested. Flame-desizing was achieved by slowly moving a long fiber tow through a torch flame.

A field-emission scanning electron microscope (FEG-SEM, LEO DSM 982, LEO Electron Microscopy Inc. Thornwood, NY) and a LaB_6 transmission electron microscope (Philips CM30 TEM, Eindhoven, Netherlands) were used for coating morphology characterization. The phases in the ZrO_2 coating were characterized by selected area electron diffraction (SAD) and convergent beam electron diffraction (CBED). The diffraction patterns were indexed using Electron Microscopy Simulation (EMS) online (http://cimesg1.epfl.ch/CIOLS/crystal1.pl). Crystallographic data from a recent review paper on the crystal structure of ZrO_2 were used in analyzing our data.[3] TEM specimens were prepared by placing fiber tows of interest between two single crystal silicon wafer pieces using an epoxy adhesive (M-Bond 610, Measurement Group, Raleigh, NC). The "sandwich" specimens were then cured for 2 h at 170°C in air and then cross-sectioned to small coupons of 0.5×2×5 mm.

The coupons were polished using a tripod-polishing technique,[4] and some of them were also ion-milled with an ion-milling machine (DuoMill™ 600, Gatan Inc., Pleasanton, CA).

A Dilor XY 800 triple stage Raman microprobe (JY, Inc., Edison, NJ) and an Innova 308C Argon ion laser (Coherent, Inc., Santa Clara, CA) operating at 514.5 nm with a 100 mW output power were used to detect the phase content of the CVD-zirconia coating at Oak Ridge National Laboratory. The laser was focused onto areas of interest with an optical objective providing a spatial resolution of 2 μm. The method for calculating the phase content was based on comparing the Raman peak heights of monoclinic and tetragonal zirconia and is described in detail in reference.[5]

III. Results

Based on initial SEM results, three specimens were selected for in-depth TEM investigation to study the morphological evolution of CVD-ZrO_2 on the surface of Hi-Nicalon fiber as a function of deposition time (5, 20, and 120 min). As shown in Figure 2a and 2b, two distinct regions were observed for the ZrO_2 coating deposited for 5 min. In some regions, the ZrO_2 coating was continuous with a thickness of ~100 nm (Figure 2a). The "continuous" regions were characterized by SAD. The rings in the diffraction pattern in Figure 2a were indexed to *c* (cubic) and/or *t* nanocrystallites, whereas the spots were assigned to larger *c* and/or *t* particles. However, no *m* phase was observed in the continuous regions.

Note that the *c* and *t* phases have very similar structures, and therefore it is generally difficult to distinguish the *c* and *t* phases based on diffraction patterns. In order to complement TEM analysis, Raman microscopy was also used for phase determination. Even though the CVD-ZrO_2 coating after the 5 min deposition was too thin to be detected by Raman microscopy,

Raman data from other CVD-ZrO_2 coatings indicated that *t* was the only phase detected. So we suppose that the phase indexed to be *c/t* by electron diffraction patterns is mainly *t* phase. For the rest of the paper, we will use the *t* notation to distinguish this phase indexed by TEM from the *m* phase.

In the other regions, the ZrO_2 coating was discontinuous with individual grains directly attached to the fiber surface. As shown in Figure 2b, the grains were ~50 nm thick and ~50 to 100 nm long along the fiber surface. Some of the grains were *t*, while the others were *m*. Figures 2c and 2d are high-resolution images of the *m* particles with all the fringes corresponding to the $(\bar{1}11)$ plane of the *m* phase. Note that the $(\bar{1}11)$ plane has the lowest surface free energy for the *m* phase.[6]

Since the *t* phase is a high-temperature phase for ZrO_2, the *t* grains could not have been transformed from the *m* phase during the CVD process at 1050°C or during cooling from the deposition temperature. This argument implies that the *t* grains should have been *t* when they were deposited at 1050°C. On the other hand, the *m* grains observed by TEM could either be *m* phase when deposited, or they could have transformed from the *t* phase during the CVD process and/or the cooling step.

Figure 3 shows TEM images of the CVD-ZrO_2 coating after the 20 min deposition. As shown in Figure 3a, delamination occurred within the ZrO_2 coating close to the fiber surface. This observation indicates that a weak interface developed within this deposition time period. In contrast, no debonding was observed between the ZrO_2 coating and the fiber or within ZrO_2 coating after the 5 min deposition. High-resolution images (Figures 3b and 3c) show that the inner ZrO_2 layer retained on the fiber side is ~50 to 100 nm thick and contains both *t* and *m* phases. It is interesting to note that the *t* (111) plane and *m* $(\bar{1}11)$ planes are almost normal to the

coating growth direction, suggesting the development of through-thickness preferred orientations. Note that these planes represent the lowest energy surfaces for their crystal structures.[6] The interface between the ZrO_2 layer and the fiber surface was sharp, indicating the absence of any major reaction there.

Based on the analysis of diffraction patterns collected at various coating locations, the amount of the *m* phase present in the ZrO_2 layer after the 20 min deposition was observed to be higher than that observed after the 5 min deposition, particularly in the outer layer that was detached from the fiber. This observation suggests that some of the *t* phase in the outer region of the coating might have been transformed to the *m* phase between 5 and 20 min during the CVD process and/or the cooling step.

Cross-sectional SEM and TEM images of the CVD-ZrO_2 coating after the 120 min deposition are shown in Figure 4. As in the case of the 20 min sample, delamination was observed within the ZrO_2 coating at a distance of ~50 to 100 nm from the fiber surface. The surface SEM images shown in Figure 5 provide additional evidence that the delamination occurred within the ZrO_2 coating. It is evident from the SEM images that the inner layer is composed of very small particles (~50 to 100 nm) deposited on the fiber surface. Above the inner layer, larger ZrO_2 grains were observed and were identified to be mostly *m* by SAD. However, at the very top surface of the ZrO_2 coating, very small *t* and *m* particles under ~50 to 100 nm were observed again, as shown in the SEM pictures in Figure 5 and the TEM images in Figure 4c. The observations suggest that ZrO_2 nuclei were continuously formed on the deposition surface throughout the 120 min period.

The Raman spectra of both the surface and the cross-section of the CVD-ZrO_2 coating after the 120 min deposition are shown in Figure 6. Only the *m* phase was detected from the

cross-section of this specimen, but the presence of the *t* phase (~13 vol%) was detected from the surface of this specimen. However, the *c* phase was not detected in either case. The difference between the two spectra is consistent with our TEM observations that the *t* phase was at the outer surface of the ZrO_2 coating and the *m* phase was mainly present in the middle region of this coating.

Figure 7 shows the failure loads of Hi-Nicalon™ fiber tows coated with the CVD-ZrO_2 as a function of deposition time. Figure 7 also compares the failure loads of coated fiber tows to those of flame-desized fiber tows. All the coated samples showed higher failure loads than the desized fiber tows. This demonstrated that the ZrO_2 coatings did not degrade fiber strength. In contrast, a CVD-SiO_2 coating severely degraded the strength of Hi-Nicalon when its thickness exceeded about 80 nm.[7] It was also interesting to observe that for two of the five 120 min specimens, the fiber tow did not fail totally within the gauge length, as some fibers showed a fiber pull-out behavior in the "matrix" formed by the epoxy. The epoxy here is used to bond the fiber tow to its plastic support.

IV. Discussion

The first major question encountered in this study is why the high temperature *t* phase of ZrO_2 was present in our CVD-ZrO_2 coating at room temperature. A brief review of phase transformations in ZrO_2 is needed before discussion of the experimental observation. The ambient-pressure phases of ZrO_2 are a *monoclinic* phase ($P2_1/c$), which is stable up to 1205°C, a *tetragonal* phase ($P4_2/nmc$) from 1205-2377°C, and a *cubic* fluorite structure ($Fm\bar{3}m$) from 2377°C to the melting point at 2710°C. The *t*-to-*m* transformation is diffusionless and martensitic and is accompanied by about 9° shear and 4.5% volume dilation.[3] The *t*-to-*m*

transformation was also reported to be accompanied by a 4.9% volume dilation at room temperature and 3.5% volume dilation at 950°C.[8] On the other hand, there is almost no volume change for the *c*-to-*t* transformation.[3]

It has been previously reported that the high-temperature *t* and *c* phases can be retained to room temperature without the use of stabilizers.[9, 10] A few mechanisms have been postulated to explain the stabilization of the high-temperature phases of ZrO_2, especially for the *t* phase. Garvie[11, 12] first proposed that the lower surface energy of the *t*-ZrO_2 is responsible for the *t* phase to be present in nanocrystalline forms at or even below room temperature. He predicted that ZrO_2 particles below 10 nm in diameter could be stabilized in the tetragonal form. Those above this critical size would be subjected to the *t*-to-*m* transformation.

According to a simple thermodynamic approach recently presented by Chraska,[13] the Gibbs free energy change due to the *t*-to-*m* phase transformation of an unconstrained spherical particle, may be expressed as:

$$\Delta G(r) = \frac{4}{3}\pi r^3 \Delta G_v + 4\pi r^2(\gamma_m - \gamma_t) \qquad (1)$$

where r is the radius of a particle, ΔG_v is the chemical energy difference for the phase transformation per unit volume of an infinite crystal, and γ_t and γ_m are the average surface free energy for the *t* and *m* phases, respectively. γ_t and γ_m have been measured by calorimetry for polycrystalline specimens to be 0.77 Jm^{-2} and 1.13 Jm^{-2}, respectively. Also, the surface free energy will not change much with temperature, and the $d\gamma_t/dT$ is only about -10^{-4} $Jm^{-2}°C^{-1}$.[14, 15] A critical value (r_c), below which the *t* phase can be stabilized, can then be determined as a function of temperature (T) by setting $\Delta G(r_c)$ equal to 0. Writing ΔG_v as a linear function of ΔH, one finds:

$$r_c = \frac{-3}{\Delta H(1 - T/T_b)}(\gamma_t - \gamma_m) \qquad (2)$$

where ΔH is the enthalpy difference between the *t* and *m* phase (-2.82×10^8 Jm^{-3}) at the equilibrium bulk transformation temperature, and T_b is the *t-m* transformation temperature for bulk ZrO_2 (1250°C).[12, 3] As shown in Figure 8, the critical size increases with increasing temperature. This phenomenon is often referred as the "size effect" in the literature.[11]

This simple model suggests that, at our typical deposition temperature of 1050°C, ZrO_2 grains with a critical radius below 35 nm (or ~70 nm in grain size) could be stable as tetragonal if the grains were nucleated directly as the tetragonal phase. However, this model should not be taken too quantitatively for comparison to our experimental observations since: (1) constraints, i.e. in the matrix or by the fiber substrate, are ignored,[16] (2) grain size distribution is not considered, and (3) the surface free energy changes at elevated temperature are not incorporated. As shown in Figure 2b, in the CVD-ZrO_2 coating after the 5 min deposition, some grains with size of ~ 50nm, which is much bigger than the calculated critical grain size 10 nm at room temperature, were still observed with TEM. Also, *t*-ZrO_2 grains with sizes bigger than 10 nm were also found in the inner CVD-ZrO_2 coating retained on fiber (Figure 3c). It is possible that the transformation of these *t*-ZrO_2 grains could be locally "constrained" by the fiber substrate.

In addition to the size and constraint effect, there are also other explanations for stabilization of the *t* and *c* phases at lower temperature including water vapor, domain boundaries, anionic vacancies favorable for *t*-nucleation, and topotactic crystallization.[13] For example, Tomaszewski, et al.[17] observed that a lower oxygen partial pressure was responsible for the metastability of undoped *c*-ZrO_2 particles dispersed in an alumina matrix.

Based on our results to date, a possible mechanism for the observed weak interface can be considered. Our observations correlate the morphological evolution of the CVD-ZrO_2 to the development of the weak interface behavior, as schematically illustrated in Figure 9.

At the very beginning of the CVD process (Figure 9a), ZrO_2 nucleates on the amorphous SiC fiber surface. Note that it takes several adatoms to form critical nuclei due to tremendous supersaturation in typical CVD conditions.[18] Once formed, some nuclei will coalesce and grow via the arrival of adatoms produced by heterogeneous chemical reactions at the deposition surface. Due to the size effect and fiber surface constraints, the initial coating layer mostly consists of *t* nanocrystals but also possibly contains some *m* particles of ~50-100 nm in some areas. Meanwhile, the formation of new ZrO_2 nuclei is continuing at the coating surface. The ZrO_2 deposited for the 5 min deposition might just have been at this stage.

As the CVD deposition proceeds, normal grain growth takes place within the ZrO_2 layer, as illustrated in Figure 9b. First, *t* nanocrystals coalesce to form larger grains, and some of them grow to the critical grain size (~70 nm from Eq. 2). This grain growth step is expected to be diffusion controlled. Above this critical size, most *t* grains martensitically transform to the *m* phase. Since the *t*-to-*m* transformation is accompanied by significant volume dilation, the ZrO_2 layer becomes compressively stressed. Once a certain degree of the transformation process is accumulated, the overall compressive stress developed in the ZrO_2 layer may be high enough to delaminate the transformed ZrO_2 region from the fiber surface during CVD and/or cooling.

The *m* grains in the delaminated side of the ZrO_2 layer continue to grow by consuming other neighboring grains in the lateral direction. At the same time, new nuclei are being formed on the deposition surface. The CVD-ZrO_2 produced after 20 min might have been at this stage. With increasing deposition time, the average gain size of the *m* phase in the delaminated layer

increases. After 120 min, the coating morphology shown in Figure 9f emerges (compare this schematic illustration to the TEM and SEM images in Figures 4 and 5).

It is evident from the TEM results that delamination consistently occurs at a distance of ~50 to 100 nm from the fiber surface and within 20 minutes. It is interesting that the delamination occurs within the ZrO_2 coating rather than the interface between the ZrO_2 and the fiber. This can be attributed to the transformation lag in the inner ZrO_2 layer, where the *t*-to-*m* phase transformation is constrained by fiber substrate. Such a constraint may lead to a larger critical size for transformation of the grains on the fiber surface. Consequently, the grains on the fiber surface transform late or only partially, as shown in Figure 3c.

Once the delamination takes place, the ZrO_2 grains in the inner layer exhibit no further significant grain growth (Figures 3 and 4). Also, the grains remaining on the fiber surface are preferentially oriented after 20 min of the deposition step and appear to reach a stagnant columnar microstructure.[19] Therefore, for these reasons, most of the *t*-ZrO_2 grains in the inner ZrO_2 layer do not grow much and consequently do not transform and delaminate even after 120 min. Meanwhile, the less physical contact between the ZrO_2 grains close to the delaminated regions also impedes the grain growth rate of those grains. Those grains are thus smaller than those deposited afterwards.

Based on the above discussion, the weak interface behavior associated with the ZrO_2 fiber coating is mainly attributed to the *t*-to-*m* phase transformation within the ZrO_2 coating during the CVD process (and/or possibly during cooling), which leads to delamination within the coating layer. So the composite behavior previously observed[2] can be explained by the delamination within ZrO_2 coating, serving as the mechanism for the apparent weak interface behavior. The CTE mismatch, which must have been involved in the evolution of the CVD-ZrO_2

coating, was also considered in this study. However, it seems that the CTE mismatch couldn't be the dominant effect controlling the weak interface behavior. If CTE mismatch is dominant, the ZrO_2 layer should shrink much more than the Hi-Nicalon fiber substrate during cooling, since ZrO_2 has the biggest CTE in the system. This shrinkage would eventually lead to the development of hoop tensile stresses in the ZrO_2 coating. Failure would then be by microcraking rather than by delamination.

To serve as a robust fiber coating for SiC/SiC ceramic matrix composites, there are other issues to be concerned with besides the weak interface and retention of fiber strength. For example, the integrity and uniformity of the fiber coating are important in terms of protecting the fiber surface from matrix infiltration by chemical vapor infiltration (CVI) or melt infiltration. In this regard, an undelaminated but compressively stressed coating might be preferred prior to the matrix infiltration. We are currently studying how to proactively control the nucleation behavior of CVD ZrO_2 and, consequently, the extent of the phase transformation in the coating layer for optimizing various interfacial properties including delamination and sliding resistance of SiC/SiC minicomposites.

V. Conclusions

Our results suggest that the *t*-to-*m* transformation within the CVD-ZrO_2 layer is most likely the key mechanism responsible for the apparent weak interface behavior previously observed with SiC/SiC minicomposite specimens containing a $SiO_2/ZrO_2/SiO_2$ multilayer coating. A simple thermodynamic model, which describes the size effect in the *t*-to-*m* phase transformation, was used to understand morphological evolution observed for the ZrO_2 layer as a function of deposition time. The morphological evolution was related to the development of a

delamination within the ZrO_2 layer. The delamination location was within the ZrO_2 layer, but ~50 to 100 nm from the fiber surface. The delamination appears to result from the following chain of events: (1) continuous formation of *t*-ZrO_2 nuclei on the deposition surface; (2) diffusion-controlled grain growth; (3) the tetragonal-to-monoclinic martensitic transformation of grains upon reaching their critical size, above which the tetragonal phase is no longer stable; and (4) development of significant compressive hoop stresses due to the volume dilation associated with the transformation. Our observations suggest that it will be of critical importance to further understand and eventually control the nucleation and grain growth behavior of CVD ZrO_2 and its phase transformation behavior for effectively assessing the potential of CVD-ZrO_2 as replacement for the BN fiber coating for SiC/SiC composites.

Acknowledgements

We are grateful to Dr. B. Greenberg at Stevens Institute of Technology for his discussion on crystallography for the EMS simulations. Michael J. Lance was supported in part by the Division of Materials Sciences and Engineering, Office of Basic Energy Sciences, Department of Energy.

References

[1] D.W. Johnson et al., "Ceramic Fibers and Coatings: Advanced Materials for the Twenty-First Century," National Materials Advisory Board, National Academy Press (1998).

[2] W.Y. Lee, Edgar Lara-Curzio, and Karren L. More, " Multilayered Oxide Interphase Concept for Ceramic-Matrix Composites," *J. Am. Ceram. Soc.*, **81**, [3] 717-20 (1998).

[3] E.H. Kisi and C.J. Howard, "Crystal Structure of Zirconia Phases and Their Inter-Relation," *Key Engineering Materials*, **153-154** 1-36 (1998).

[4] S. J. Klepeis, J. P. Benedict and R. M. Anderson, "A Grinding/Polishing Tool for TEM Sample Preparation," *Mat. Res. Soc. Proc.*, **115**. 179-184 (1988).

[5] M. J. Lance, J. A. Haynes, M. K. Ferber and W. R. Cannon, "Monoclinic Zirconia Distributions in Plasma-Sprayed Thermal Barrier Coatings," *Journal of Thermal Spray Technology*, **9** [1], 68-72 (2000).

[6] A. Christensen, and EA Carter, "First Principles Study of the Surfaces of Zirconia," *Phys. Rev. B*, **58**, 8050 (1998).

[7] J. I. Lee, H. Li, M. Libera, W. Y. Lee, H. Wang, and G. N. Morscher, "Role of First SiO_2 Layer in a Multilayer $SiO_2/ZrO_2/SiO_2$ Fiber Coating for SiC/SiC Ceramic Composites," Advances in Ceramic Matrix Composites VI, Ceramic Transactions, **124**, edited by J.P. Singh, Narottam O. Bansal, and Ersan Ustundag, 102nd Annual Meeting of The American Ceramic Society, St. Louis, Missouri, 15-26 (2001).

[8] W. M. Kricen, "Possible Alternative Transformation Toughners to Zirconia: Crystallographic Aspects," *J. Am. Ceram. Soc.*, **71** [12] 1021-30 (1988).

[9] J. Minet, F. Langlais, and R. Naslain, " On The Chemical Vapour Deposition of Zirconia from $ZrCl_4$-H_2-Ar Gas Mixture: II An Experimental Approach," *J. Less-Common Metals*, **132**, 273-287 (1987).

[10] M. Morstein, Imre Pozsgai, and Nicholas D. Spencer, *Chem. Vap. Deposition*, **5**, No. 4 151-158 (1999).

[11] R. C. Garvie, "The Occurrence of Metastable Tetragonal Zirconia as a Crystallite Size Effect," *J. Phys. Chem.*, **69**, 1238-1243 (1965).

[12] R. C. Garvie, "Stabilization of the Tetragonal Structure in Zirconia Microcrystals," *J. Phys. Chem.*, **82**, 218-224 (1978).

[13] Tomas Chraska, Alexander H. King, and Christopher C. Berndt, "On the Size-Dependent Phase Transformation in Nanoparticulate Zirconia," *Materials Science and Engineering*, **A286**, 169-178 (2000).

[14] H. F. Holmes, E. L. Fuller, Jr., and R. B. Gammage, "Heats of Immersion in the Zirconium Oxide-Water System," *J. Phys. Chem.*, **76**, 1497-1502 (1972).

[15] D. T. Livey and P. Murray, " Surface Energies of Solid Oxides and Carbides," *J. Am. Ceram. Soc.*, **29**, 363-372 (1956).

[16] F. F. Lange, "Transformation Toughening: Part 1 Size Effects Associated with the Thermodynamics of Constrained Transformation," *J. Mater. Sci.*, **17**, 225-234 (1982).

[17] Henryk Tomaszewski and Krzysztof Godwod, "Influence of Oxygen Partial Pressure on the Metastability of Undoped Zirconia Dispersed in Alumina Matrix," *J. Europ. Ceram. Soc.*, **15**, 17-23 (1995).

[18] J. Bloem, "Nucleation and Growth of Silicon by CVD," *J. Crystal Growth*, **50**, 581-604 (1980).

[19] C. V. Thompson, "Grain Growth in Thin Films," *Ann. Rev. Mater. Sci.*, **20**, 245-268 (1990).

List of Figures

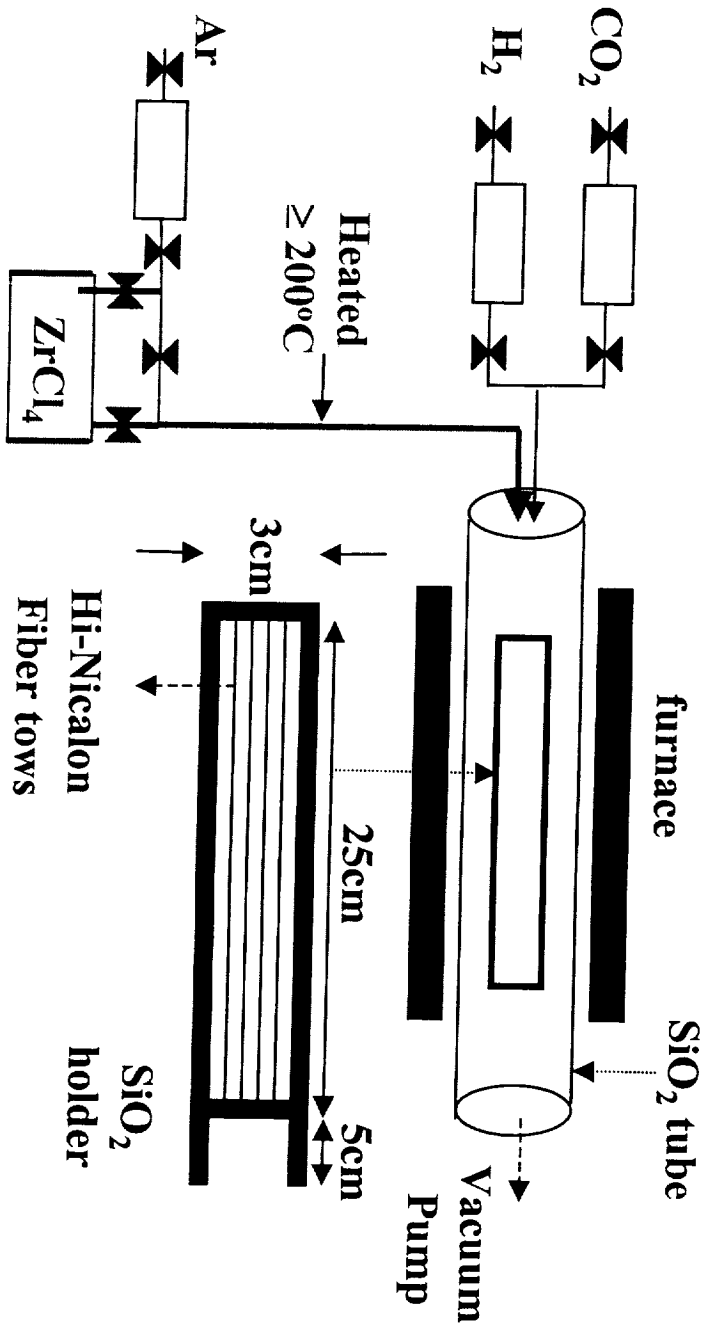
Mass
Flowmeters
CO_2
H_2
Ar
Heated
≥ 200°C
$ZrCl_4$
Resistance
furnace
SiO_2 tube
Vacuum
Pump
3cm
25cm
5cm
Hi-Nicalon
Fiber tows
SiO_2
holder

Fig. 1

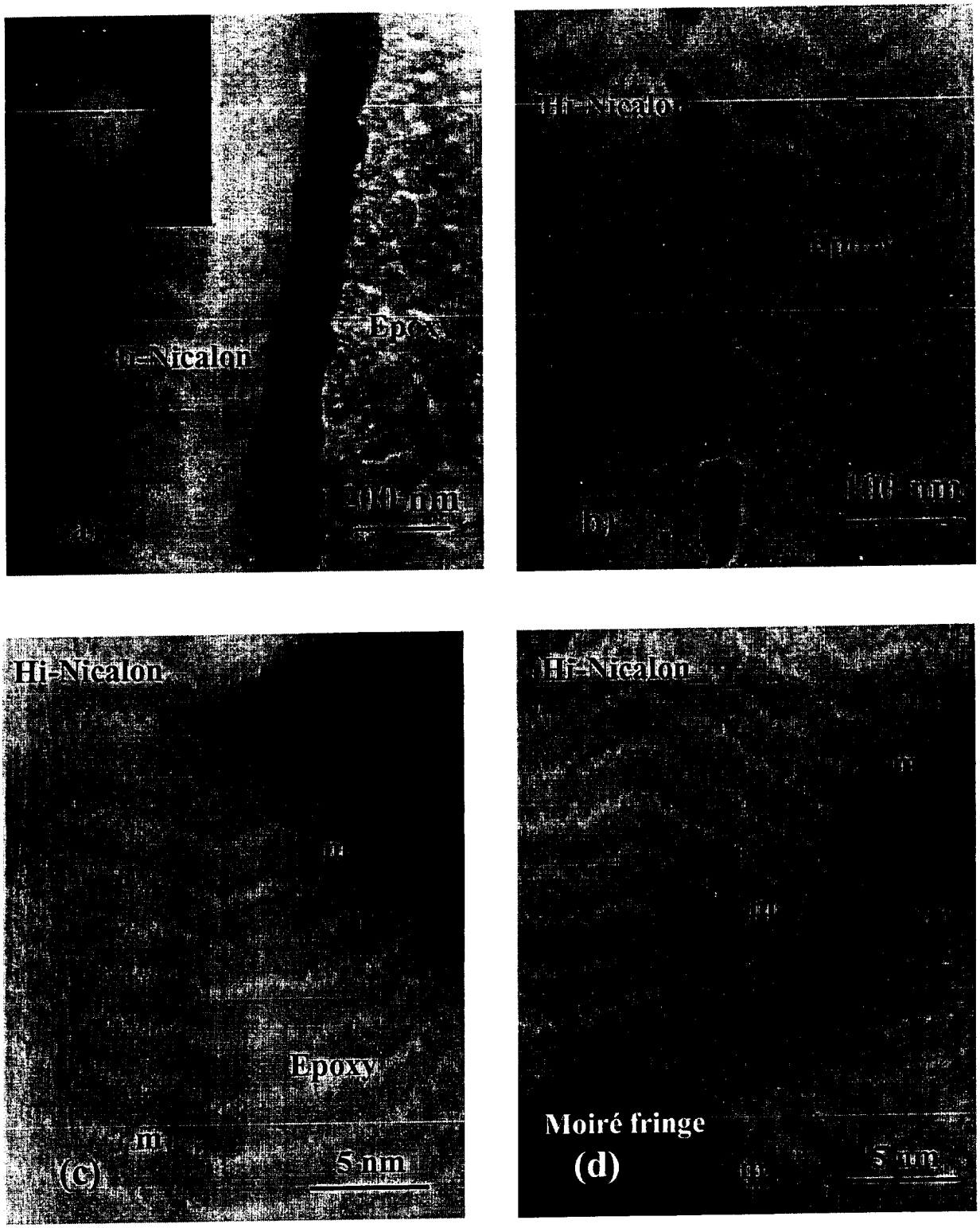

Fig. 2

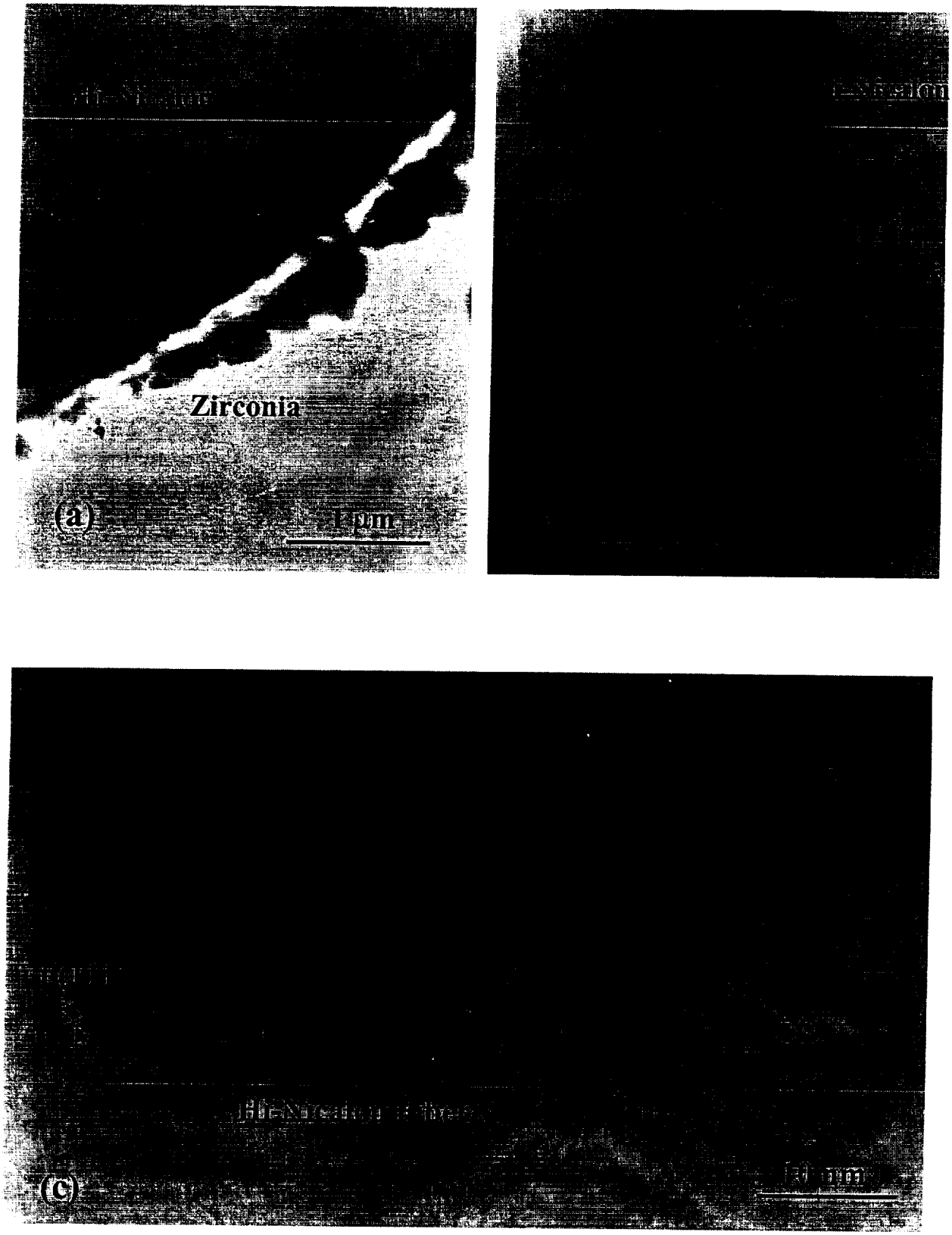

Fig. 3

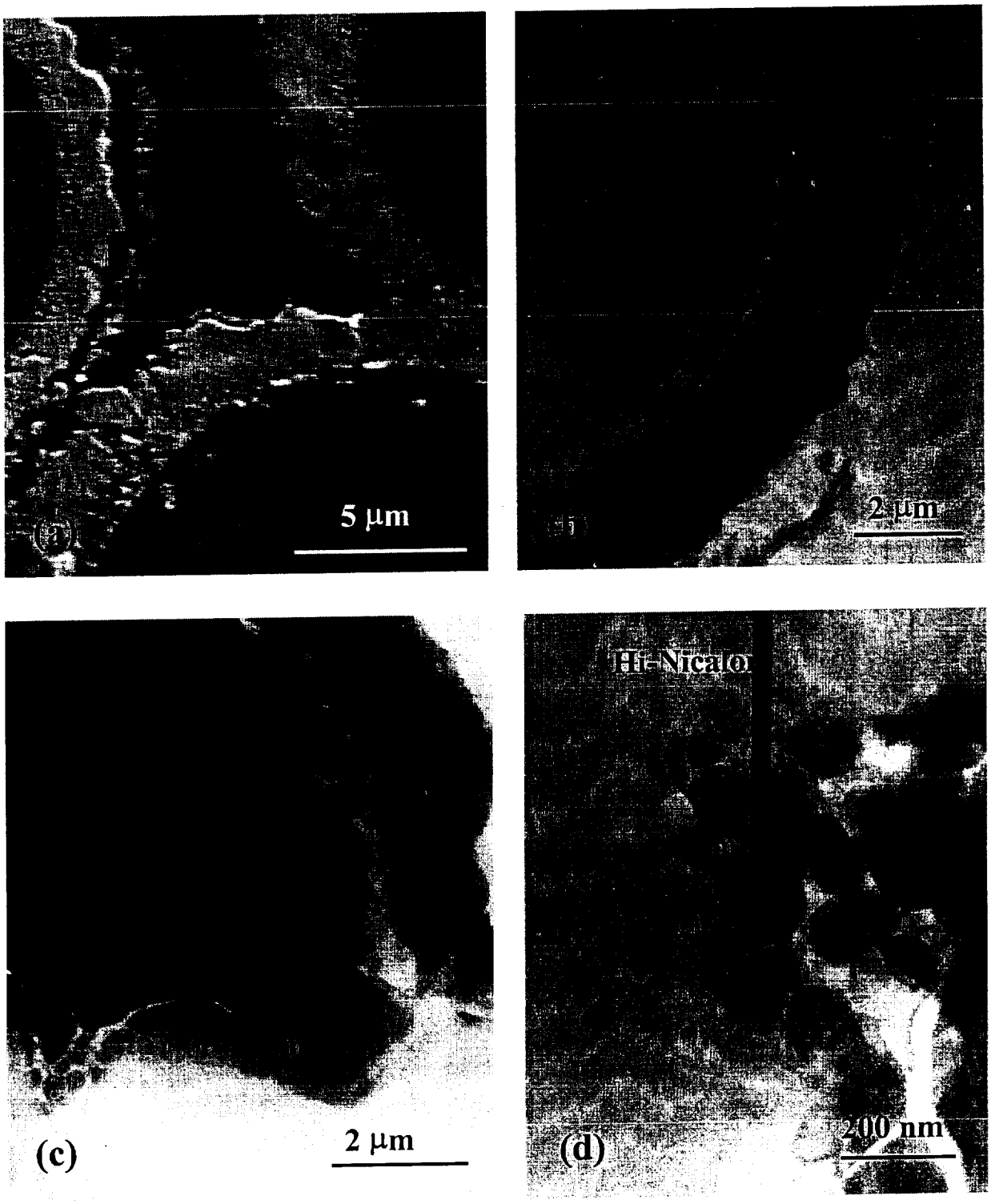

Fig. 4

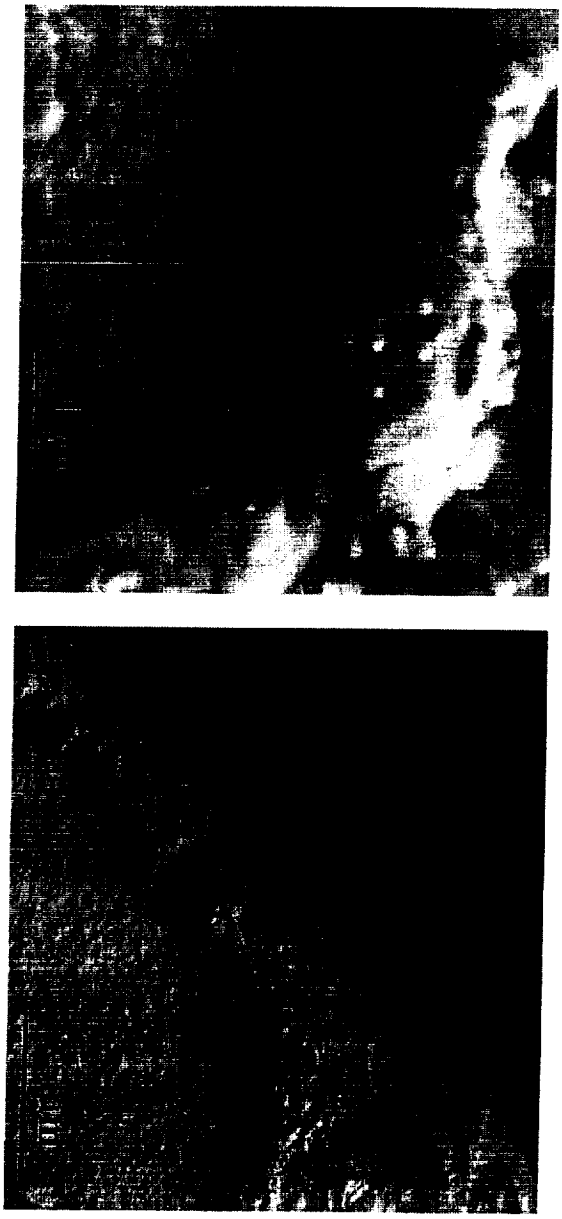

Fig. 5

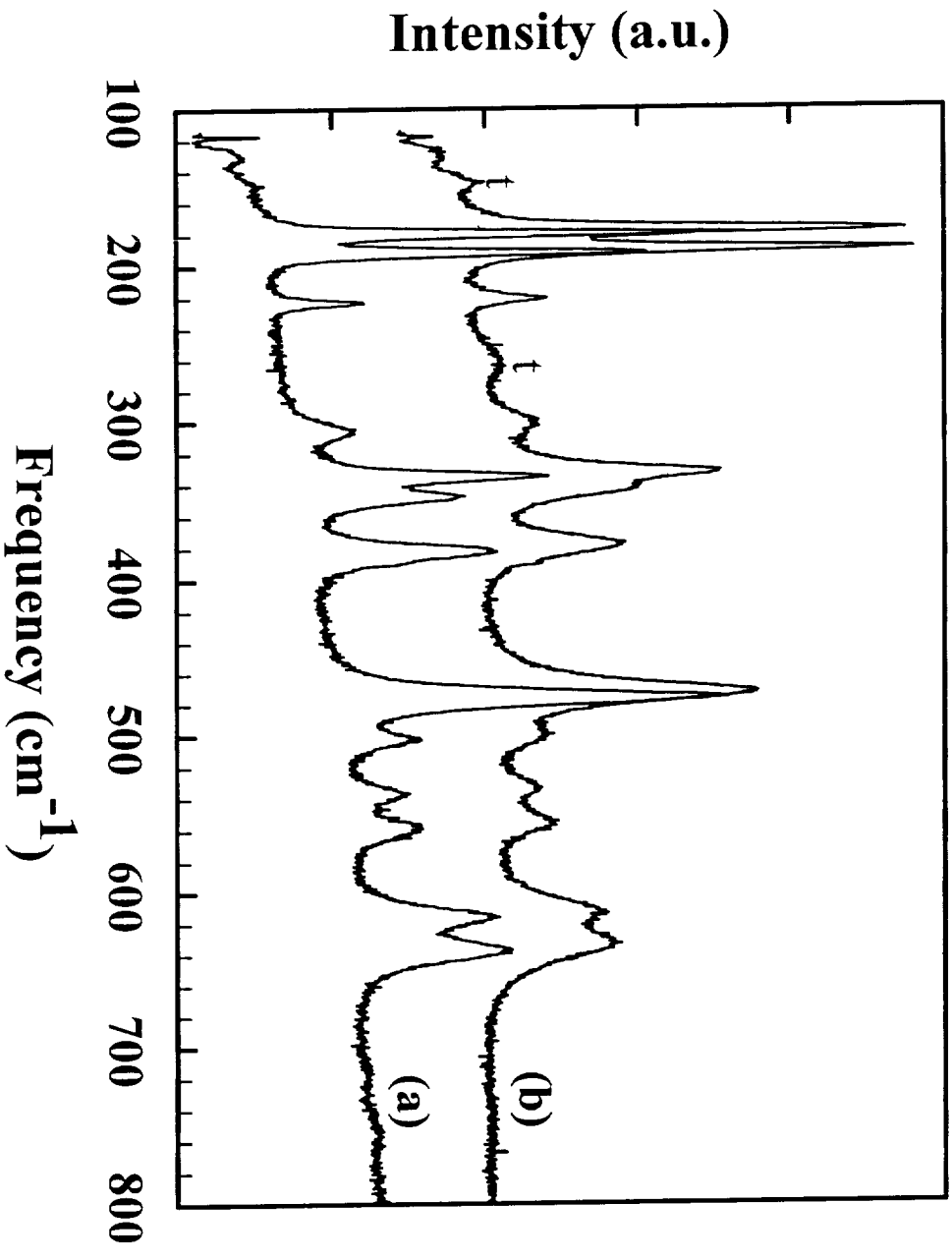
Intensity (a.u.)
Frequency (cm-1)
100
200
300
400
500
600
700
800
t
t
(a)
(b)

Fig. 6

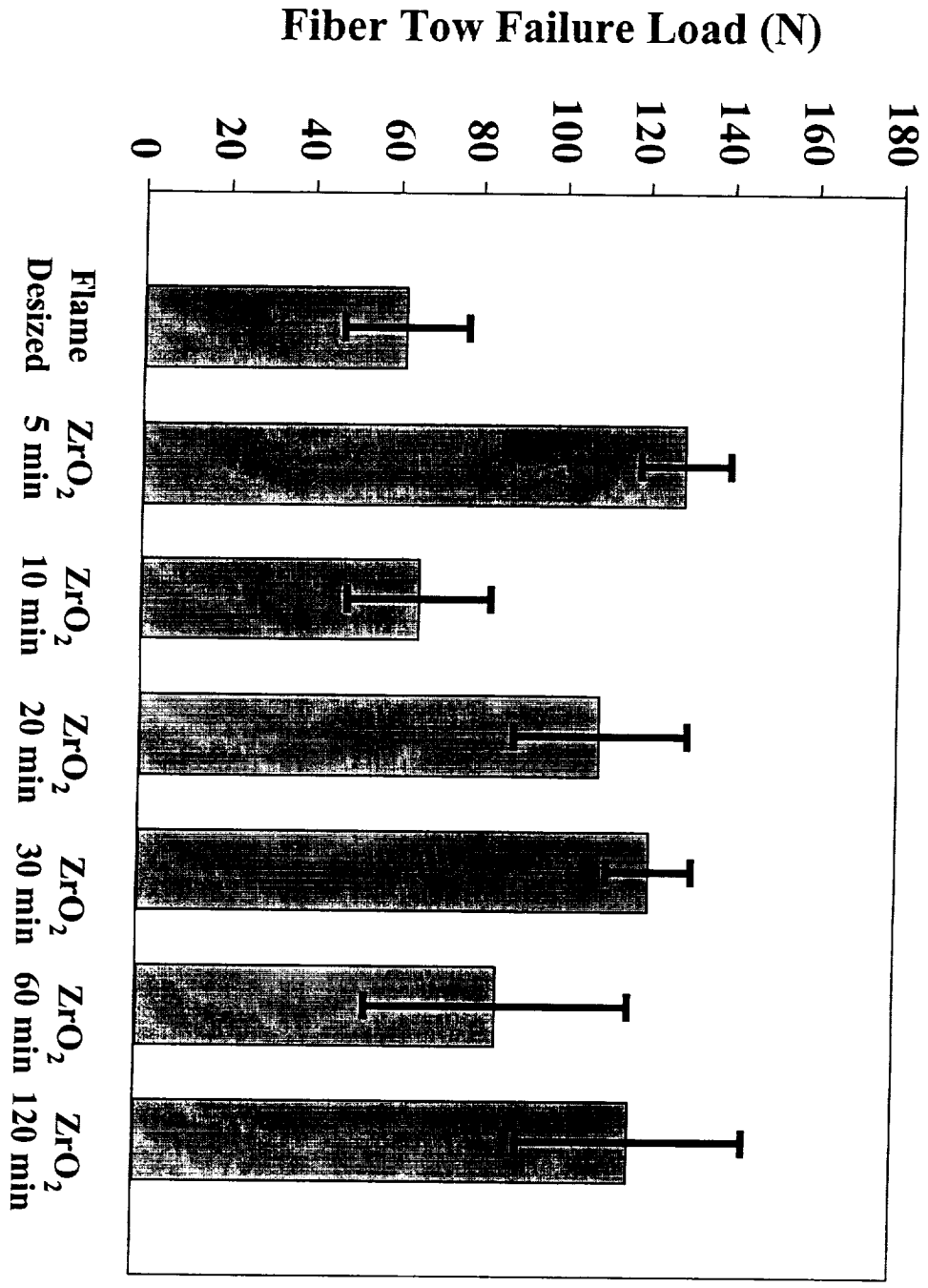
Fiber Tow Failure Load (N)
0
20
40
60
80
100
120
140
160
180
Flame Desized
ZrO2 5 min
ZrO2 10 min
ZrO2 20 min
ZrO2 30 min
ZrO2 60 min
ZrO2 120 min

Fig. 7

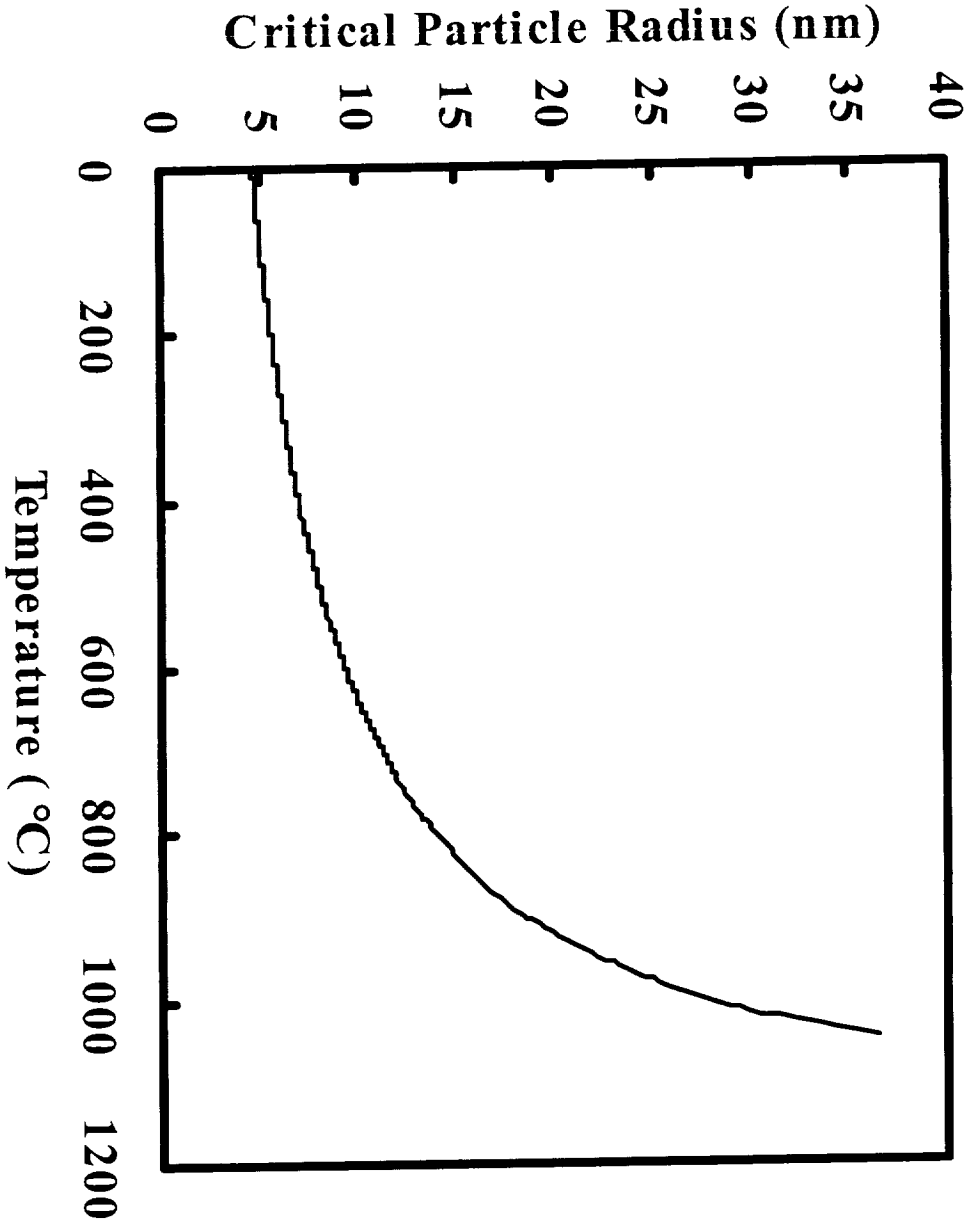
Critical Particle Radius (nm)
0
5
10
15
20
25
30
35
40
Temperature (°C)
0
200
400
600
800
1000
1200

Fig. 8

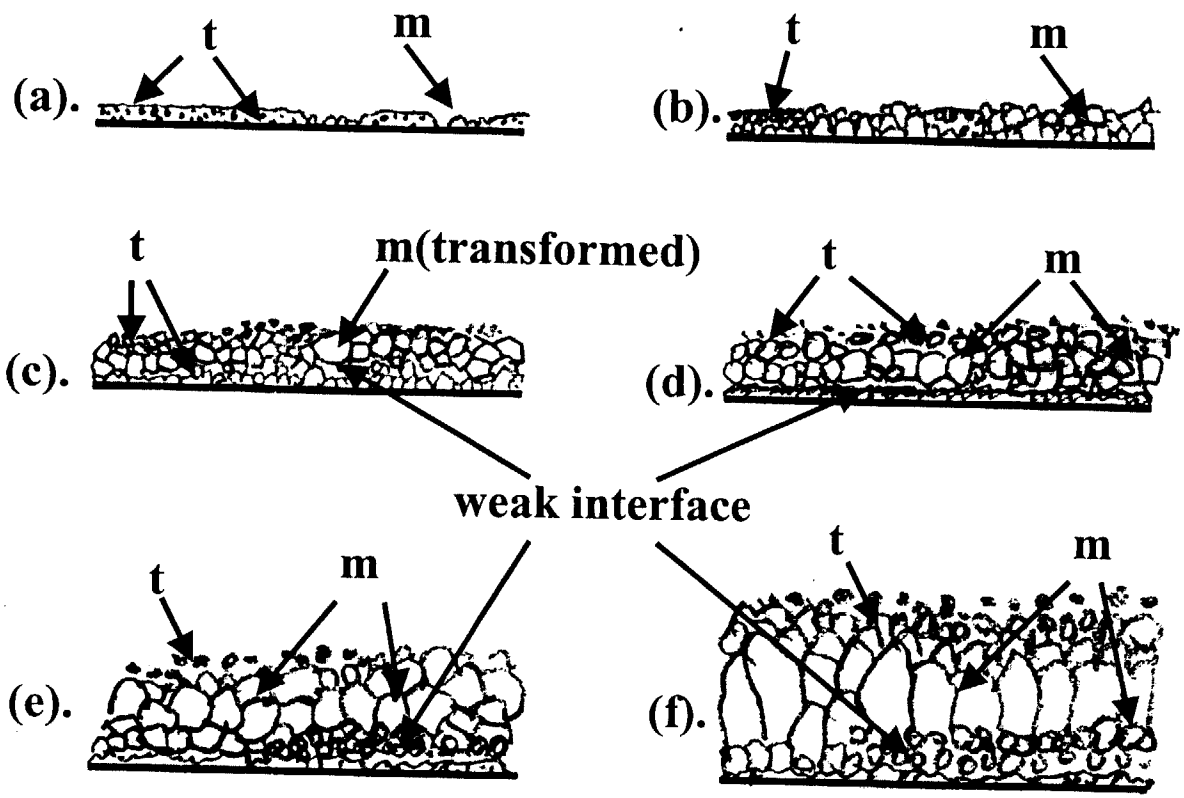

Fig. 9